

## Article

# Structural, Magnetic, and Optical Properties of Mn<sup>2+</sup> Doping in ZnO Thin Films

Monika Sharma <sup>1,\*</sup>, Kakoli Bera <sup>1</sup>, Ruby Mishra <sup>2</sup> and Alka V. Kuanr <sup>3</sup>

<sup>1</sup> Department of Physics, Deshbandhu College, University of Delhi, New Delhi 110019, India; kakolibera@gmail.com

<sup>2</sup> Department of Chemistry, Deshbandhu College, University of Delhi, New Delhi 110019, India; rubymishradu@gmail.com

<sup>3</sup> Shaheed Rajguru College of Applied Science for Women, Jhilmil Colony, University of Delhi, New Delhi 110096, India; alkavohra07@gmail.com

\* Correspondence: msharma@db.du.ac.in; Tel.: +91-8383811692

**Abstract:** Mn<sub>x</sub>Zn<sub>1-x</sub>O thin films (x = 0%, 1%, 3%, and 5%) were grown on corning glass substrates using sol-gel technique. Single-phase hexagonal wurtzite structure was confirmed using X-ray diffraction. Raman analysis revealed the presence of Mn content with an additional vibrational mode at 570 cm<sup>-1</sup>. The surface morphology of the samples was observed by scanning electron microscopy which suggested that the grain size increases with an increase in Mn concentration. The optical bandgap increases with increasing Mn concentration due to a significant blueshift in UV-visible absorption spectra. The alteration of the bandgap was verified by the I-V measurements on ZnO and Mn-ZnO films. The various functional groups in the thin films were recorded using FTIR analysis. Magnetic measurements showed that Mn<sub>x</sub>Zn<sub>1-x</sub>O films are ferromagnetic, as Mn induces a fully polarised state. The effect of Mn<sup>2+</sup> ions doping on Mn<sub>x</sub>Zn<sub>1-x</sub>O thin films was investigated by extracting various parameters such as lattice parameters, energy bandgap, resistivity, and magnetisation. The observed coercivity is about one-fifth of the earlier published work data which indicates the structure is soft in nature, having less dielectric/magnetic loss, and hence can be used as ultra-fast switching in spintronic devices.

**Keywords:** ZnO; thin films; magnetic properties; energy band-gap



**Citation:** Sharma, M.; Bera, K.; Mishra, R.; Kuanr, A.V. Structural, Magnetic, and Optical Properties of Mn<sup>2+</sup> Doping in ZnO Thin Films. *Surfaces* **2021**, *4*, 268–278. <https://doi.org/10.3390/surfaces4040022>

Academic Editors: Antonio Caggiano and Gaetano Granozzi

Received: 29 September 2021

Accepted: 28 October 2021

Published: 31 October 2021

**Publisher's Note:** MDPI stays neutral with regard to jurisdictional claims in published maps and institutional affiliations.



**Copyright:** © 2021 by the authors. Licensee MDPI, Basel, Switzerland. This article is an open access article distributed under the terms and conditions of the Creative Commons Attribution (CC BY) license (<https://creativecommons.org/licenses/by/4.0/>).

## 1. Introduction

In recent years, ZnO-based metal oxide semiconductors have drawn significant attention due to their versatility and tuneable optical, electrical, and magnetic properties. These materials can be synthesised in different physical forms such as nanoparticles, single crystals thick, and thin films [1–5]. Among these, thin films form an important and useful structure for various applications such as gas sensors, optoelectronic devices, transparent electrodes for solar cells, and as a catalyst [6–9]. It is also being considered as a potential candidate in the new frontiers of research such as spintronics [10]. Diluted magnetic semiconductors (DMSs), generally obtained by substituting a small amount of transition metal (TM) in oxide semiconductors, are expected to show ferromagnetism at room temperature due to the interaction between the spins of the carriers and the localised moments of TM impurities [11–13]. The ferromagnetic behaviour of TM-doped ZnO thin films has been extensively studied due to their potential to control both spin and electric charge which makes these materials suitable for spintronic applications at or above room temperature. In particular, Mn can be used as a transition metal dopant for obtaining ferromagnetic ordering due to its high magnetic ordering [14,15]. However, very few reports studied the influence of Mn<sup>2+</sup> doping on magnetic properties in detail [16–18]. Gallegos et al. have studied structural, electronic, and magnetic properties of ZnO and Mn-doped ZnO theoretically by first-principles calculations based on density functional theory (DFT) [19].

Hexagonal wurtzite crystal structure of ZnO with  $\text{Zn}^{2+}$  and  $\text{O}^{2-}$  ions tetrahedrally coordinated and stacked along *c*-axis alternatively exhibit large exciton binding energy (60 meV) and high optical transparency (3.3 eV). Mn-doped ZnO has been reported recently by many researchers for showing electrical, magnetic, and optical properties simultaneously [20–23].  $\text{Mn}_x\text{Zn}_{1-x}\text{O}$  shows room temperature ferromagnetism which makes it a promising candidate for spintronic applications. However, there are few reports emphasising the ferromagnetic and electrical properties of the Mn-doped ZnO thin films. TM-doped ZnO thin films have been synthesised by various deposition techniques such as spray pyrolysis, reactive ion-assisted evaporation, molecular beam epitaxy, RF magnetron sputtering, chemical vapour deposition, and sol-gel [24–29]. Among these, the sol-gel technique is the simplest and most cost-effective method that enables the formation of different structures by changing the experimental conditions using the same composition of the material [30].

In this work, we investigated the effect of  $\text{Mn}^{2+}$  ions doping in ZnO thin films. We varied the manganese concentration in ZnO films from 0% to 5%. The structural, morphological, optical, and magnetic properties were explored in these thin films using X-ray diffraction (XRD), Raman spectroscopy, Fourier transform infrared spectroscopy (FTIR), scanning electron microscopy (SEM), UV-visible spectrometer, and vibrating sample magnetometer (VSM), respectively. The present investigation has revealed that crystallite size and optical bandgap increase with the increase in Mn concentration in ZnO thin films. Room temperature ferromagnetism was observed in Mn-doped ZnO thin films, which can be a potential candidate specifically for spintronic applications. I–V measurements demonstrated that the energy separation between the uppermost layer of the valence band and unoccupied states in the conduction band increases with Mn doping in ZnO thin films.

## 2. Experimental Procedure

The sol-gel technique was employed for the synthesis of 0%, 1%, 3%, and 5%  $\text{Mn}_x\text{Zn}_{1-x}\text{O}$  thin films. Zinc acetate dihydrate [ $\text{Zn}(\text{CH}_3\text{COO})_2 \cdot 2\text{H}_2\text{O}$ , SRL-76205] and manganese acetate dihydrate [ $\text{Mn}(\text{CH}_3\text{COO})_2 \cdot 2\text{H}_2\text{O}$ , SRL-78017] from SRL with purity > 99% were used as the zinc, and manganese sources, respectively, and 2-mithoxyethanol (DME-GRM8601, Himedia, Maharashtra, India) [ $\text{C}_3\text{H}_8\text{O}_2$ ] and mono-ethanolamine (MEA-GRM10183, Himedia) [ $\text{C}_2\text{H}_7\text{NO}$ ] were used as the solvent and stabiliser, respectively. All the chemicals were of analytical grade and used without further purification. In addition, 0.5 M zinc acetate dihydrate was used as a starting material. The Zinc precursor was weighed on the 6-digit accuracy weighing balance with the four parts of the same quality mass. The manganese acetate dihydrate as a dopant was added to them, and the atomic mole ratio of dopant Mn to Zn was varied at different concentrations of 0%, 1%, 3%, and 5%, respectively. These four mixtures were then dissolved at room temperature in four amounts in a homogeneous mixture of MEA and DME solution. The MEA served as a stabiliser. The molar ratios of MEA to zinc acetate were maintained at 1:1. A homogeneous, and clear solution was obtained by stirring the final mixture vigorously at 70 °C for 2 h using a magnetic stirrer. Further, it was held for aging at room temperature for one day to receive the desirable sol. For thin film deposition, the corning glass substrates ( $5 \times 5 \text{ cm}^2$ ) were cleaned first with de-ionised water by ultrasonication for 5 min, followed by ultrasonication in isopropanol alcohol for 10 min. The cleaned substrates were then coated with a homogeneous solution using a spin coater at 3000 rpm and 30 s time interval. After first spinning, the substrates were preheated at 300 °C for 5 min to evaporate the solvent in the films. The spin-coating and preheating processes were repeated 20 times for the formation of uniform thin films. The estimated thickness of the films at present conditions was around 10  $\mu\text{m}$  [31]. These coated films were annealed at 500 °C in the muffle furnace under an air atmosphere for 2 h and then cooled to room temperature.

The structural properties of the films were investigated at room temperature by using Miniflex 600 X-ray diffractometer from Rigaku with monochromatic Cu  $K\alpha$  radiation ( $\lambda = 1.5418 \text{ \AA}$ ) at 40 kV and 15 mA in the diffraction angle ( $2\theta$ ) range of 20°–60°, with a step size of 0.02° and a scanning speed of 5°/min. We used Match software, available online,

for the phase analysis of XRD data. The Raman spectroscopic analysis was performed at room temperature to investigate the vibrational modes using EnSpectr Raman spectrometer in the range 150–800  $\text{cm}^{-1}$  using a green laser source with a power of 300 mW and a wavelength of 532 nm. The surface morphology of the films was studied using scanning electron microscopy (SEM; JSM-IT200) at 10,000 magnification. For obtaining the SEM images, a thin gold layer (~30 nm) was coated on the film surface. The samples were then mounted on the SEM holders. The Fourier transform infrared (FTIR; Thermo Scientific NICOLET iS50, ABX) transmittance measurements were performed in the range from 400 to 4000  $\text{cm}^{-1}$  with a resolution of 2  $\text{cm}^{-1}$ . UV–visible spectrophotometer was used to measure the optical absorption and transmittance spectra, and optical bandgap was derived using Tauc's plot of transmission spectra on T90+ UV–vis spectrometer. The magnetic measurements performed by vibrating sample magnetometer (VSM-Cryogenic Ltd., London, UK) were used to obtain saturation magnetisation, coercivity, and remanence. The magnetic field was applied parallel to the film plane surface (in-plane geometry). I–V measurements were performed using Palmsen4 with applied voltage from  $\pm 5$  V. Prior to measurements, silverpoint contacts were made on the top surface of the films.

### 3. Results and Discussion

The X-ray diffraction pattern of ZnO and Mn-doped ZnO samples annealed at 500 °C are shown in Figure 1. It is confirmed from the XRD pattern that all the films showed a single crystalline phase with no additional impurity of Mn metal and oxides. From the diffraction peaks, it is clear that all the samples showed a wurtzite structure with (002) preferred orientation which matches with the JCPDS file No. 79-206 for ZnO. The Mn-doped samples also showed other reflection planes at (100) and (101) of negligible intensity. The crystallite sizes of all the samples were determined using Debye–Scherrer formula [32].

$$D = \frac{k\lambda}{\beta \cos\theta} \quad (1)$$

where  $k$  denotes the Scherrer constant of proportionality and can be considered to be 0.9,  $\lambda$  denotes the wavelength of the incident X-ray radiation and for  $\text{CuK}\alpha$ ,  $\lambda = 1.5418 \text{ \AA}$ ,  $\beta$  corresponds to the full-width half maxima of interested peak, and  $\theta$  is the Bragg angle. It is observed that the crystallite size increased from 36.2 nm to 51.1 nm for an increase of 5% Mn in ZnO thin films. This can be attributed due to the large ionic radius of Mn, as compared with Zn causes the grain size to increase. The lattice parameters  $a$  and  $c$  of the wurtzite structure of ZnO can be calculated using the relation in [33].

$$a = \sqrt{\frac{1}{3} \frac{\lambda}{\sin\theta}} \quad (2)$$

$$c = \frac{\lambda}{\sin\theta} \quad (3)$$

For the (002) plane, the lattice parameters were observed to be  $a = 3.245 \text{ \AA}$  and  $c = 5.227 \text{ \AA}$  which is similar to the reported work [33,34]. We observed that the lattice parameters increase with the Mn doping in ZnO thin films. Table 1 shows the lattice parameters obtained for ZnO thin film and 5% Mn-doped ZnO thin film samples.

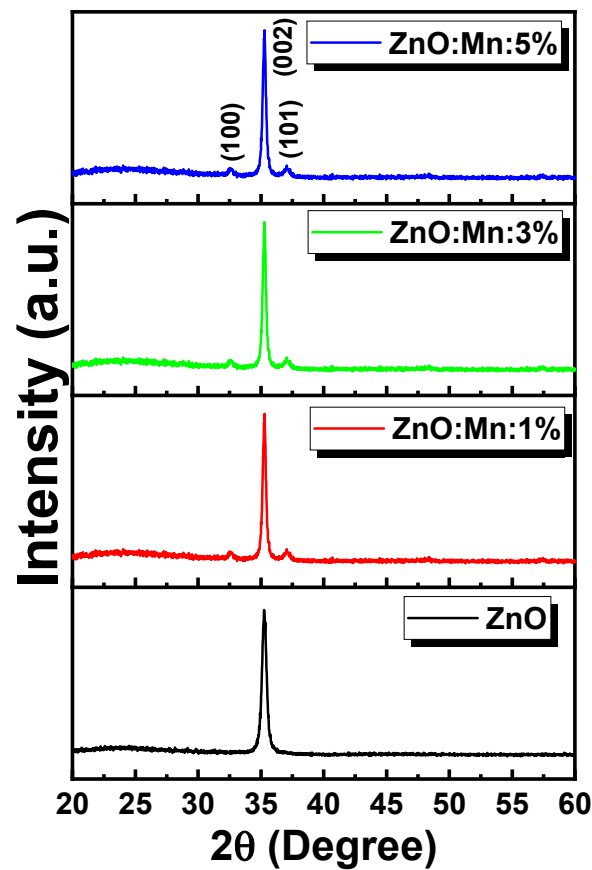


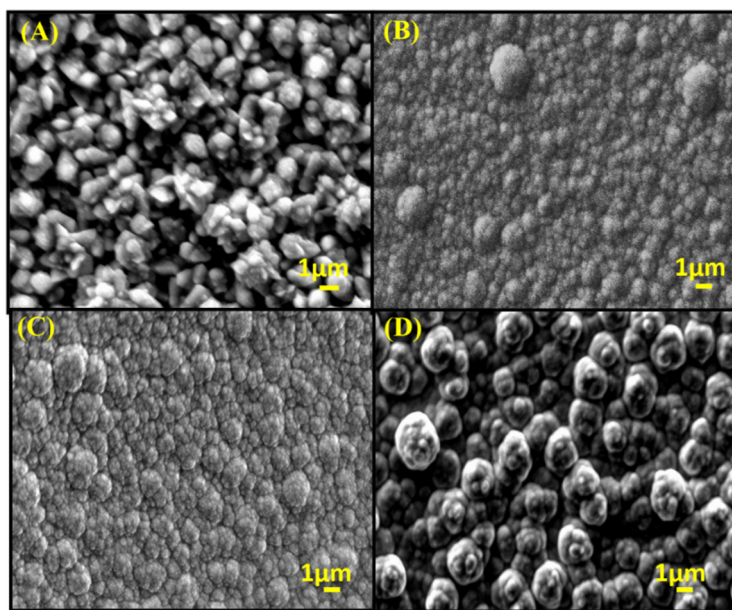
Figure 1. XRD pattern of ZnO and Mn-doped ZnO thin films.

Table 1. Cell parameters and energy bandgap of undoped ZnO thin film and 5% Mn-doped ZnO thin film.

Parameters	ZnO Thin Film	ZnO:Mn:5% Thin Film
$a = b$ (Å)	3.245	3.253
$c$ (Å)	5.227	5.223
$c/a$	1.6108	1.606
Volume (Å <sup>3</sup> )	47.67	47.86
Crystallite Size (nm)	36.2	51.1

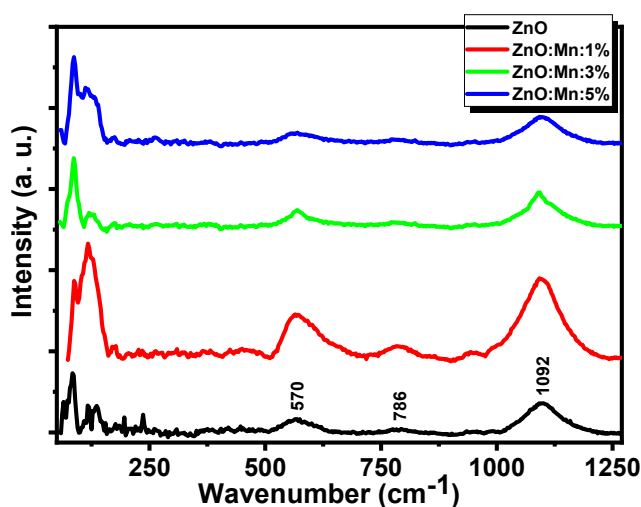
A comparison of our experimental results with the first-principles calculation simulated data shows that ZnO bond length practically was not affected by the incorporation of the Mn atom. The obtained results of a comparison of the cell parameters reflect that the Mn-doped ZnO had a small change with respect to the ZnO system, which is in accordance with the DFT calculations [19]. The parameter  $a$  increased about 0.3% (from 3.12 Å to 3.13 Å), while the  $c$  parameter was reduced 0.6% from first-principles calculations [19], whereas our experimental results show that  $a$  increased about 0.25%, and  $c$  parameter was reduced 0.07%.

Figure 2 shows the scanning microscope images of all the deposited thin films. It is clearly visible from the SEM spectra that the films were uniformly deposited on the corning glass substrates, and the grain size increased with the increase in Mn concentration in the ZnO films.



**Figure 2.** Scanning microscope image of Mn-doped ZnO thin films  $Mn_xZn_{1-x}O$ : (A) 0%; (B) 1%; (C) 3%; (D) 5%.

The Raman spectra demonstrate the effect of Mn concentration on the vibrational and microscopic properties of  $Mn_xZn_{1-x}O$  thin films. Figure 3 shows the Raman peaks at  $570\text{ cm}^{-1}$  which corresponds to A1(LO) mode due to the generation of Zn vacancy to be filled with Mn dopant. A significant redshift was observed in the Mn-doped ZnO thin films as the ZnO wurtzite A1 vibrational mode occurred at  $580\text{ cm}^{-1}$  which could be the result of oxygen vacancy and zinc interstitials defect states. The peak centred at  $1092\text{ cm}^{-1}$  corresponded to the glass substrate and C-C vibration mode present in the organic radical ( $CH_3COO^-$ ) of  $Mn_xZn_{1-x}O$  thin films, respectively. It can further be related to the combination of Raman scattering and luminescence [35–37]. From Figure 3, it is obvious that the characteristics modes centred at  $570\text{ cm}^{-1}$  and  $1092\text{ cm}^{-1}$  were sharp and intense.



**Figure 3.** Raman Spectra of  $Mn_xZn_{1-x}O$  thin films deposited for different Mn concentrations annealed at  $500\text{ }^\circ\text{C}$ .

The presence of functional groups such as Mn-O, Zn-O, and -OH was observed using Fourier transform infrared spectra (FTIR) measurements, as shown in Figure 4. The incorporation of Mn in ZnO was confirmed by the variation in the peaks' position and

their intensity. The band in the range of 400–600  $\text{cm}^{-1}$  corresponded to the stretching vibration of the Zn-O and (Zn, Mn)-O. The OH vibrational mode due to absorption of water molecules at the sample surface occurred at absorption band around the wavenumber 3400  $\text{cm}^{-1}$ . The peak at 2250–2400  $\text{cm}^{-1}$  corresponded to  $\text{CO}_2$  modes. The absorption peak at 1540  $\text{cm}^{-1}$  corresponded to antisymmetric stretching mode C=O bonding. The antisymmetric stretching mode of Mn-O vibration mode occurred at wavenumber 880  $\text{cm}^{-1}$  [33]. The observed FTIR results are in good agreement with the earlier reported works [38,39].

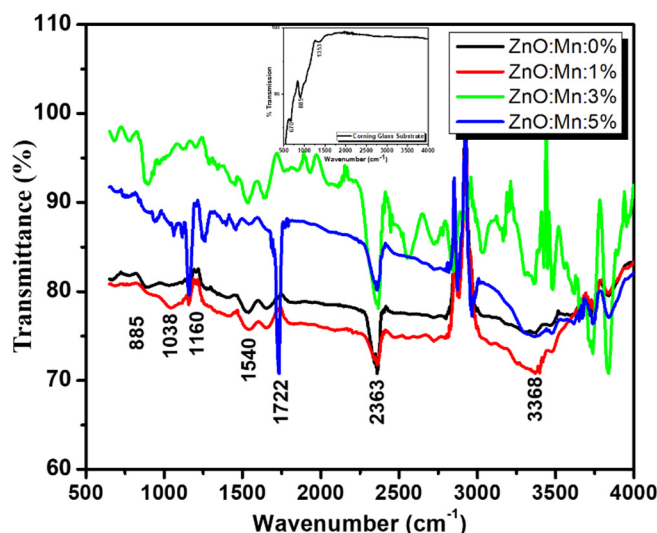


**Figure 4.** FTIR spectra for  $\text{Mn}_x\text{Zn}_{1-x}\text{O}$  thin films with different Mn doping concentrations (inset: FTIR spectrum of corning glass substrate).

The UV–visible absorption spectra of  $\text{Mn}_x\text{Zn}_{1-x}\text{O}$  thin films were taken in the wavelength range 300–900 nm. It is observed that all the films were transparent with small absorption in the visible region of the electromagnetic spectrum and the absorption peaks show redshift with the addition of Mn dopant. Figure 5A reveals the corresponding transmittance spectra of the deposited films. It is clear from the transmittance spectra that the films had smooth reflecting surface which can be attributed to low scattering loss at the surface and also due to the appearance of interference fringes that originated from the light reflected between air–film and film–substrate interface. The decrease in transmittance with increasing Mn concentration can be attributed due to the formation of lattice defects at ZnO interstitial sites. In order to achieve the optical bandgap of deposited thin films, we used Tauc’s plot analysis [40–42] as follows:

$$\alpha h\nu = A(h\nu - E_g)^n \quad (4)$$

where  $\alpha$  is the absorption coefficient which depends upon the thickness of the film,  $h$  is the Planck constant,  $A$  is proportionality constant, and  $n = 1/2$  for direct bandgap semiconductors. The absorption coefficient can be estimated by using [43],

$$\alpha = \left(\frac{1}{d}\right) \ln\left(\frac{1}{T}\right) \quad (5)$$

where  $T$  is the transmittance and  $d$  is the film’s thickness. The Tauc’s plot for all the films is shown in Figure 5B, and the optical bandgap was determined by extrapolating the graph on the energy axis, as shown by the dashed line in Figure 5B. It was observed that the bandgap increased from 3.23 eV to 3.28 eV with increasing Mn doping concentration. The blueshift in the bandgap can be attributed to the replacement of  $\text{Zn}^{2+}$  ions by  $\text{Mn}^{2+}$  ions in the ZnO lattice, causing the energy separation between the uppermost layer of the valence band and unoccupied states in the conduction band [44]. Further, Shaaban et al. reported

that the bandgap of Mn-doped ZnO thin films is increased since the bandgap of MnO (4.2 eV) is greater than that of ZnO [45]. The bandgap also increases with the increase in particle size which can be explained as the bulk defects induce a delocalisation of the conduction band edge and create vacancies in electronic energy causing a blueshift of the absorption spectra [46].

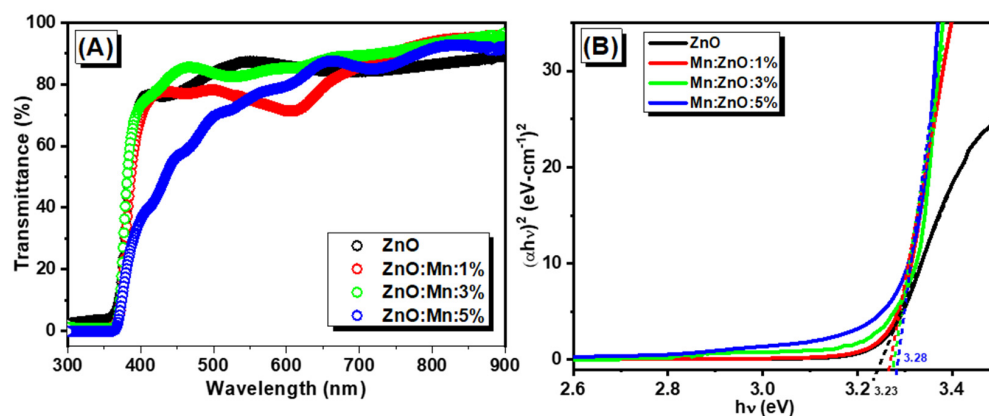


**Figure 5.** UV-visible spectra of  $Mn_xZn_{1-x}O$  thin films: (A) transmittance spectra as a function of wavelength; (B)  $(\alpha h\nu)^2$  as a function of photon energy ( $h\nu$ ) for different Mn concentration samples.

The magnetic hysteresis loop of the  $Mn_xZn_{1-x}O$  thin films is shown in Figure 6. The graph demonstrates that with the addition of Mn concentration (1%, 3%, and 5%), the films became ferromagnetic in nature. The ZnO film is observed to be nonmagnetic, in agreement with the null magnetic moment, due to a deficiency of unpaired electrons. With the increase in Mn dopant in ZnO films, the ferromagnetism increased which may be due to the increase in oxygen vacancies, resulting in a bound magnetic polaron [17,18]. The introduction of Mn in the ZnO induced a magnetic moment. This is due to five unpaired 3d electrons in the outermost shell. Our experimental findings are consistent with the behaviour of the density-of-states calculations [19].

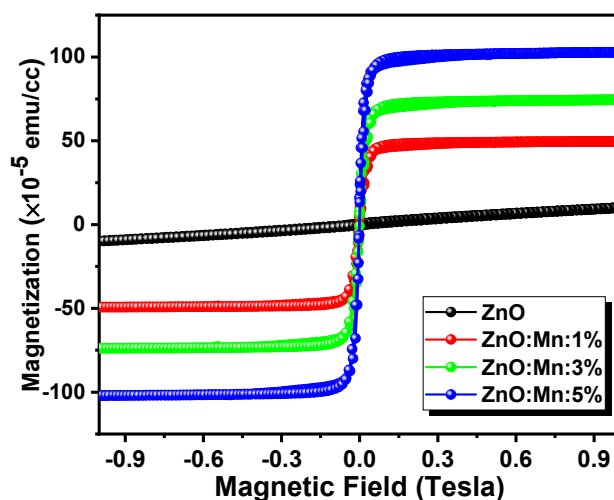


**Figure 6.** Magnetic hysteresis loop of  $Mn_xZn_{1-x}O$  thin films.

The magnetic saturation, coercivity, and remanence of the  $Mn_xZn_{1-x}O$  thin films are tabulated in Table 2. The saturation magnetisation increased with the increase in Mn concentration in ZnO thin films. A closer look into the magnetism of the undoped ZnO and Mn-doped ZnO reveals that the undoped ZnO had an equal number of spin-up and spin-down states. When Mn was incorporated into ZnO, a difference of five electrons between the states appeared in the Mn-ZnO system. This caused an increase in a magnetic moment

of  $5 \mu_B$ , as obtained through DFT calculation [19]. We observed the coercivity to be one-fifth of reported data [16]. This implies that our studied thin films were much softer magnetically which indicates much lower dielectric/magnetic losses. The observed coercivity can be correlated to much narrower ferromagnetic linewidth, indicating much smaller Gilbert damping and hence can be used as faster magnetically switching devices [47]. Our results were compared with previous reported works in Table 3.

**Table 2.** Magnetic properties of Mn-doped ZnO thin films at different concentrations of 0%, 1%, 3%, and 5%.

Sample Name	Saturation Magnetisation ( $\times 10^{-3}$ emu/cc)	Coercivity (Oe)	Remanence ( $\times 10^{-5}$ emu/cc)
ZnO	Non-magnetic	-	-
ZnO:Mn:1%	0.50	9.90	3.55
ZnO:Mn:3%	0.74	9.95	5.3
ZnO:Mn:5%	1.03	10.75	11.5

**Table 3.** Comparison of observed parameters with other studies in the literature for 5% Mn-doped ZnO thin films.

S. No.	Parameters	Present Work	Reported Work	References
1.	Crystallite size (nm)	51.1	42	[17,22]
2.	Optical bandgap (eV)	3.28	3.22	[23]
3.	Saturation magnetisation	$1.03 \times 10^{-3}$ emu/cc	$11 - 26 \times 10^{-4}$ emu/g	[18,22]
4.	Coercivity (Oe)	10.75	50.5	[16]

Figure 7 represents the I–V measurements of undoped and Mn-doped ZnO thin films with an applied voltage of  $\pm 5$  V. It is observed from the plot that for a specific voltage with the increase in Mn doping, the current decreased which corresponded to an increase in resistivity. This is consistent with the increase in bandgap with the increase in Mn concentration, as the energy separation between the uppermost layer of the valence band and unoccupied states in the conduction band increased with Mn doping in ZnO thin films [44,48].

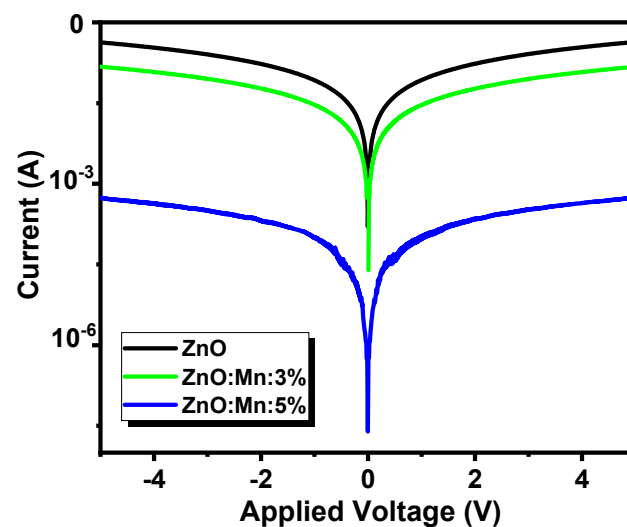


**Figure 7.** I–V plot of  $Mn_xZn_{1-x}O$  thin films.

#### 4. Conclusions

We successfully fabricated  $Mn_xZn_{1-x}O$  thin films on the corning glass substrates by sol-gel technique. The structural analysis ratified the wurtzite structure of ZnO films with preferred orientation along the c-axis. The crystallite size and grain size were observed to increase with increasing Mn concentration. The UV-visible analysis revealed a blueshift with an increase in Mn dopant which may be due to oxygen vacancy and zinc interstitials defect states. The optical bandgap increased with the increase in Mn concentration. The increase in bandgap was verified through I-V measurements, with an increase in resistance in Mn-ZnO films. Typical ferromagnetic behaviour was observed for  $Mn_xZn_{1-x}O$  thin films due to five unpaired 3d electrons in the outermost shell. Enhancement of magnetisation in Mn-doped ZnO thin films indicated its potential applications in spintronic devices. The low coercivity makes them suitable for magnetically ultrafast switching devices.

**Author Contributions:** Conceptualization, M.S., K.B. and A.V.K.; Formal analysis, M.S. and R.M.; Investigation, M.S. and R.M.; Methodology, R.M.; Supervision, A.V.K.; Visualization, K.B.; Writing—original draft, M.S.; Writing—review & editing, K.B. and A.V.K. All authors have read and agreed to the published version of the manuscript.

**Funding:** This research received no external funding.

**Institutional Review Board Statement:** Not applicable.

**Informed Consent Statement:** Not applicable.

**Data Availability Statement:** Not applicable.

**Conflicts of Interest:** The authors declare no conflict of interest.

#### References

1. Samanta, A.; Goswami, M.N.; Mahapatra, P.K. Magnetic and electric properties of Ni-doped ZnO nanoparticles exhibit diluted magnetic semiconductor in nature. *J. Alloy. Compd.* **2018**, *730*, 399–407. [[CrossRef](#)]
2. Bandyopadhyay, A.; Gupta, N.; Nath, M.; Chakraborty, S.; Sutradhar, S. Magnetic properties of Mn doped ZnO: A Monte Carlo simulation analysis. *Vacuum* **2021**, *183*, 109786. [[CrossRef](#)]
3. Ahmad, N.; Khan, S.; Ansari, M.M.N. Optical, dielectric and magnetic properties of Mn doped SnO<sub>2</sub> diluted magnetic semiconductors. *Ceram. Int.* **2018**, *44*, 15972–15980. [[CrossRef](#)]
4. Khan, R.; Fashu, S.; Rehman, Z.U.; Khan, A.; Rahman, M.U. Structure and magnetic properties of (Co, Mn) co-doped ZnO diluted magnetic semiconductor nanoparticles. *J. Mater. Sci. Mater. Electron.* **2018**, *29*, 32–37. [[CrossRef](#)]
5. Nagaraja, K.K.; Pramodini, S.; Kumar, A.S.; Nagaraja, H.S.; Poornesh, P.; Kekuda, D. Third-order nonlinear optical properties of Mn doped ZnO thin films under cw laser illumination. *Opt. Mater.* **2013**, *35*, 431–439. [[CrossRef](#)]
6. Sankar Ganesh, R.; Durgadevi, E.; Navaneethan, M.; Patil, V.L.; Ponnusamy, S.; Muthamizhchelvan, C.; Kawasaki, S.; Patil, P.S.; Hayakawa, Y. Low temperature ammonia gas sensor based on Mn-doped ZnO nanoparticle decorated microspheres. *J. Alloy. Compd.* **2017**, *721*, 182–190. [[CrossRef](#)]
7. Diaconu, M.; Schmidt, H.; Hochmuth, H.; Lorenz, M.; Benndorf, G.; Lenzner, J.; Spemann, D.; Annette, S.; Nielsen, K.-W.; Esquinazi, P.; et al. UV optical properties of ferromagnetic Mn-doped ZnO thin films grown by PLD. *Thin Solid Film.* **2005**, *486*, 117–121. [[CrossRef](#)]
8. Sindhu, H.S.; Rajendra, B.V.; Hebbar, N.D.; Kulkarni, S.D.; Babu, P.D. Defect induced white-light emission from Mn-doped ZnO films and its magnetic properties. *J. Lumin.* **2018**, *199*, 423–432. [[CrossRef](#)]
9. Senol, S.D.; Yalcin, B.; Ozugurlu, E.; Arda, L. Structure, microstructure, optical and photocatalytic properties of Mn-doped ZnO nanoparticles. *Mater. Res. Express* **2020**, *7*, 015079. [[CrossRef](#)]
10. Siddheswaran, R.; Medlín, R.; Jeyanthi, C.E.; Raj, S.G.; Mangalaraja, R.V. Structural, morphological, optical and magnetic properties of RF sputtered Co doped ZnO diluted magnetic semiconductor for spintronic applications. *Appl. Phys. A* **2019**, *125*, 1–9. [[CrossRef](#)]
11. Sharma, P.K.; Dutta, R.K.; Pandey, A.C.; Layek, S.; Verma, H.C. Effect of iron doping concentration on magnetic properties of ZnO nanoparticles. *J. Magn. Magn. Mater.* **2009**, *321*, 2587–2591. [[CrossRef](#)]
12. Dietl, T.; Ohno, O.H.; Matsukura, A.F.; Cibert, J.; Ferrand, E.D. Zener model description of ferromagnetism in zinc-blende magnetic semiconductors. *Science* **2000**, *287*, 1019–1022. [[CrossRef](#)] [[PubMed](#)]
13. Fert, A. Origin, development, and future of spintronics (Nobel lecture). *Angew. Chem. Int. Ed.* **2008**, *47*, 5956–5967. [[CrossRef](#)]
14. Risbud, A.S.; Spaldin, N.A.; Chen, Z.Q.; Stemmer, S.; Seshadri, R. Magnetism in polycrystalline cobalt-substituted zinc oxide. *Phys. Rev. B* **2003**, *68*, 205202. [[CrossRef](#)]

15. Theodoropoulou, N.; Misra, V.; Philip, J.; LeClair, P.; Berera, G.P.; Moodera, J.S.; Satpati, B.; Som, T. High-temperature ferromagnetism in Zn<sub>1-x</sub>Mn<sub>x</sub>O semiconductor thin films. *J. Magn. Magn. Mater.* **2006**, *300*, 407–411. [[CrossRef](#)]
16. Yang, S.; Zhang, Y. Structural, optical and magnetic properties of Mn-doped ZnO thin films prepared by sol-gel method. *J. Magn. Magn. Mater.* **2013**, *334*, 52–58. [[CrossRef](#)]
17. Boukhari, A.; Deghfel, B.; Mahroug, A.; Amari, R.; Selmi, N.; Kheawhom, S.; Mohamad, A.A. Thickness effect on the properties of Mn-doped ZnO thin films synthesis by sol-gel and comparison to first-principles calculations. *Ceram. Int.* **2021**, *47*, 17276–17285. [[CrossRef](#)]
18. Saleem, M.; Siddiqi, S.A.; Atiq, S.; Anwar, M.S.; Riaz, S. Room temperature magnetic behavior of sol-gel synthesized Mn doped ZnO. *Chin. J. Chem. Phys.* **2010**, *23*, 469. [[CrossRef](#)]
19. Gallegos, M.V.; Luna, C.R.; Peluso, M.A.; Damonte, L.C.; Sambeth, J.E.; Jasen, P.V. Effect of Mn in ZnO using DFT calculations: Magnetic and electronic changes. *J. Alloy. Compd.* **2019**, *795*, 254–260. [[CrossRef](#)]
20. Hao, Y.-M.; Lou, S.-Y.; Zhou, S.-M.; Yuan, R.-J.; Zhu, G.-Y.; Li, N. Structural, optical, and magnetic studies of manganese-doped zinc oxide hierarchical microspheres by self-assembly of nanoparticles. *Nanoscale Res. Lett.* **2012**, *7*, 1–9. [[CrossRef](#)]
21. Sharma, P.; Gupta, A.; Rao, K.V.; Owens, F.J.; Sharma, R.; Ahuja, R.; Guillen, J.M.O.; Johansson, B.; Gehring, G.A. Ferromagnetism above room temperature in bulk and transparent thin films of Mn-doped ZnO. *Nat. Mater.* **2003**, *2*, 673–677. [[CrossRef](#)]
22. Bououdina, M.; Omri, K.; El-Hilo, M.; El Amiri, A.; Lemine, O.M.; Alyamani, A.; Hlil, E.K.; Lassri, H.; El Mir, L. Structural and magnetic properties of Mn-doped ZnO nanocrystals. *Phys. E Low-Dimens. Syst. Nanostruct.* **2014**, *56*, 107–112. [[CrossRef](#)]
23. Omri, K.; El Ghoul, J.; Lemine, O.M.; Bououdina, M.; Zhang, B.; El Mir, L. Magnetic and optical properties of manganese doped ZnO nanoparticles synthesized by sol-gel technique. *Superlattices Microstruct.* **2013**, *60*, 139–147. [[CrossRef](#)]
24. Nagaraja, K.K.; Kumar, A.S.; Nagaraja, H.S. Aluminum doped ZnO thin films by RF sputtering of coaxial ZnO and Al targets. *AIP Conf. Proc. Am. Inst. Phys.* **2011**, *1391*, 743–745.
25. Kawamoto, N.; Fujita, M.; Tatsumi, T.; Horikoshi, Y. Growth of ZnO on Si substrate by plasma-assisted molecular beam epitaxy. *Jpn. J. Appl. Phys.* **2003**, *42*, 7209. [[CrossRef](#)]
26. Chikoidze, E.; Dumont, Y.; Jomard, F.; Gorochoy, O. Electrical and optical properties of ZnO: Mn thin films grown by MOCVD. *Thin Solid Film.* **2007**, *515*, 8519–8523. [[CrossRef](#)]
27. Ashour, A.; Kaid, M.A.; El-Sayed, N.Z.; Ibrahim, A.A. Physical properties of ZnO thin films deposited by spray pyrolysis technique. *Appl. Surf. Sci.* **2006**, *252*, 7844–7848. [[CrossRef](#)]
28. Li, X.; Zhu, X.; Jin, K. Study on structural and optical properties of Mn-doped ZnO thin films by sol-gel method. *Opt. Mater.* **2020**, *100*, 109657. [[CrossRef](#)]
29. Sivalingam, D.; Gopalakrishnan, J.B.; Rayappan, J.B.B. Structural, morphological, electrical and vapour sensing properties of Mn doped nanostructured ZnO thin films. *Sens. Actuators B Chem.* **2012**, *166*, 624–631. [[CrossRef](#)]
30. Keskenler, E.F.; Doğan, S.; Turgut, G.; Gürbulak, B. Evaluation of structural and optical properties of Mn-doped ZnO thin films synthesized by sol-gel technique. *Metall. Mater. Trans. A* **2012**, *43*, 5088–5095. [[CrossRef](#)]
31. Mufti, N.; Arista, D.; Diantoro, M.; Fuad, A.; Taufiq, A. The Effect of Thickness of ZnO Thin Films on Hydrophobic Self-Cleaning Properties. In *IOP Conference Series: Materials Science and Engineering*; IOP Publishing: Bristol, UK, 2017; Volume 202, p. 012006.
32. Patterson, A.L. The Scherrer formula for X-ray particle size determination. *Phys. Rev.* **1939**, *56*, 978. [[CrossRef](#)]
33. Mote, V.D.; Dargad, J.S.; Purushotham, Y.; Dole, B.N. Effect of doping on structural, physical, morphological and optical properties of Zn<sub>1-x</sub>Mn<sub>x</sub>O nano-particles. *Ceram. Int.* **2015**, *41*, 15153–15161. [[CrossRef](#)]
34. Shinde, V.R.; Gujar, T.P.; Lokhande, C.D.; Mane, R.S.; Han, S.-H. Mn doped and undoped ZnO films: A comparative structural, optical and electrical properties study. *Mater. Chem. Phys.* **2006**, *96*, 326–330. [[CrossRef](#)]
35. Simandan, I.-D.; Sava, F.; Buruiana, A.-T.; Burducea, I.; Becherescu, N.; Mihai, C.; Velea, A.; Galca, A.-C. The Effect of the Deposition Method on the Structural and Optical Properties of ZnS Thin Films. *Coatings* **2021**, *11*, 1064. [[CrossRef](#)]
36. Strelchuk, V.; Kolomys, O.; Rarata, S.; Lytvyn, P.; Khyzhun, O.; Chey, C.O.; Nur, O.; Willander, M. Raman submicron spatial mapping of individual Mn-doped ZnO nanorods. *Nanoscale Res. Lett.* **2017**, *12*, 1–11. [[CrossRef](#)] [[PubMed](#)]
37. Baghdad, R.; Kharroubi, B.; Abdiche, A.; Bousmaha, M.; Bezzerrouk, M.A.; Zeinert, A.; El Marssi, M.; Zellama, K. Mn doped ZnO nanostructured thin films prepared by ultrasonic spray pyrolysis method. *Superlattices Microstruct.* **2012**, *52*, 711–721. [[CrossRef](#)]
38. Aksoy, S.; Caglar, Y. Synthesis of Mn doped ZnO nanopowders by MW-HTS and its structural, morphological and optical characteristics. *J. Alloy. Compd.* **2019**, *781*, 929–935. [[CrossRef](#)]
39. Khalid, R.; Alhazaa, A.N.; Khan, M.A.M. Synthesis, characterization and properties of Mn-doped ZnO nanoparticles. *Appl. Phys. A* **2018**, *124*, 1–8. [[CrossRef](#)]
40. Rahman, F. Effect of nickel substituted on the structural and optical properties of ZnO nanoparticles. *Int. J. Adv. Res. Sci. Eng.* **2015**, *4*, 1.
41. Siddheswaran, R.; Jeyanthi, C.E.; Thangaraju, K.; Mangalaraja, R.V. Columnar structure growth of Mn-doped ZnO (MZO) thin films by radio frequency co-sputtering and studies on films properties. *Mater. Technol.* **2020**, 1–7. [[CrossRef](#)]
42. Kant, R.; Sharma, D.; Bansal, A.; Singh, R. Structural, optical and dielectric properties of Al/Mn doped ZnO nanoparticles, a comparative study. *Mater. Technol.* **2020**, 1–8. [[CrossRef](#)]
43. Xie, Q.; Liu, X.; Liu, H. Fastly steady UV response feature of Mn-doped ZnO thin films. *Superlattices Microstruct.* **2020**, *139*, 106391. [[CrossRef](#)]

44. Coulter, J.B.; Birnie, D.P., III. Assessing Tauc plot slope quantification: ZnO thin films as a model system. *Phys. Status Solidi B* **2018**, *255*, 1700393. [[CrossRef](#)]
45. Shaaban, E.R.; El-Hagary, M.; Emam-Ismail, M.; Matar, A.; Yahia, I.S. Spectroscopic ellipsometry and magneto-transport investigations of Mn-doped ZnO nanocrystalline films deposited by a non-vacuum sol-gel spin-coating method. *Mater. Sci. Eng. B* **2013**, *178*, 183–189. [[CrossRef](#)]
46. Gautam, S.K.; Sapkota, B.; Bhujel, A.; Bhattarai, S. Estimation of Particle Size and Band Gap of Zinc Oxide Nanoparticle Synthesized by Chemical Precipitation Method. *J. Nepal Chem. Soc.* **2020**, *41*, 46–50. [[CrossRef](#)]
47. Nallusamy, S.; Nammalvar, G. Enhancement of ferromagnetism in Thiol functionalized Mn doped ZnO thin films. *Mater. Res. Express* **2018**, *5*, 026418. [[CrossRef](#)]
48. Coey, J.M.D.; Wongsaprom, K.; Alaria, J.; Venkatesan, M. Charge-transfer ferromagnetism in oxide nanoparticles. *J. Phys. D Appl. Phys.* **2008**, *41*, 134012. [[CrossRef](#)]